Supporting information

Schreml et al. 10.1073/pnas.1006945108

SI Materials and Methods

Dye Leaching and Particle Leakage. To investigate dye leaching out of particles, 5 mg FITC-aminocellulose (AC) and ruthenium(II) tris-(4,7-diphenyl-1,10-phenanthroline)-polyacrylonitrile [$Ru(dpp)_3$-PAN] were suspended in 5 mL each Millipore water (MembraPure Astacus) or Ringer's solution (B. Braun AG). Suspensions were continuously shaken for 24 h; 2 mL suspension were centrifuged (10 min at 8,400 × *g*). Supernatants were additionally filtered (200-nm cutoff syringe filter; Whatman) to separate potentially leached dye molecules and particles. We studied both the original particle suspensions and the filtered supernatants in an Aminco-Bowman AB2 luminescence spectrometer (Thermo Spectronic). Spectra of the supernatants were recorded two times, one time with the same gain as used to record spectra of the suspensions (600/800 V) and one time with full detector gain (1,275 V) to detect traces of dyes in the solutions.

Leakage of particles out of the sensor foil was investigated by incubating pH sensor foils in Ringer's solution and Millipore water, respectively. Sensor foils (surface = 2 cm^2) were placed in 2 mL respective liquids and shaken for 24 h. The sensors were removed, and the solutions were investigated in the luminescence spectrometer (full detector gain = 1,275 V). Pure Ringer's solution and Millipore water served as blank controls.

Time Response, Spectra, and Photostability. Time traces (λ_{ex} = 460 nm, λ_{em} = 530 nm, 8-nm slits) of multiple defined pH variations (pH 3–10, single pH steps) were acquired on an Aminco-Bowman AB2 luminescence spectrometer (Thermo Spectronic). Response time was defined as the time interval between the change of the buffer solution and a steady-state result. We used Britton Robinson buffers (50 mM; composed of 16.67 mM H_3BO_3, 16.67 mM H_3PO_4, 16.67 mM acetic acid in distilled water). Absorbance and luminescence (λ_{ex} = 460 nm, 4-nm slits) spectra were obtained using the same setup. We processed data with locally weighted scatterplot smoothing (LOESS). Photostability experiments were carried out on sensor foils with either FITC-AC or $Ru(dpp)_3$-PAN using the imaging setup described in the text. Relative luminescence intensities of both dyes were examined (1,000 measurement cycles) under varying pH (50 mM Britton Robinson buffers, pH 3 and 9) and oxygen (0% and 20%) values in a calibration chamber at 30 °C. Additional experiments on the operational time of the pH sensor foils were carried out by determining the luminescence intensity ratio *R* over 1,000 measurements for 0%, 10%, and 20% oxygen at pH 3, 5, 7, and 9, respectively.

Cytotoxicity. Human epidermal keratinocytes (HKs; Invitrogen) were cultured until confluence in keratinocyte growth medium with supplement (kGMS). HKs were detached using collagenase type 2 (0.1 U·mL^{-1}; Roche Diagnostics) and resuspended in kGMS. HKs (passage 3) in kGMS were seeded (2.5 × 10^3 cells·$well^{-1}$) in 96-well flat-bottom microtiter plates (Costar) and cultured (37 °C, 95% humidity, 5% CO_2) for 3 d. kGMS was renewed or replaced with FITC-AC or $Ru(dpp)_3$-PAN in kGMS (0.1, 0.5, or 1.0 μg·mL^{-1}), and HKs were incubated for 48 h. For fluorescence microscopy, we seeded HKs (passage 5) in six-well flat-bottom microtiter plates (Costar).

Fibroblast growth medium with supplement (fGMS) for L929 fibroblasts (CCL I fibroblast, NCTC clone 929; American Type Culture Collection) consisted of DMEM supplemented with 5% vol/vol FBS, 2 mM L-glutamine, 2.2 mg·mL^{-1} sodium bicarbonate, penicillin, and streptomycin (Lonza). L929 (passage 4) were cultured until confluence on 75-cm^2 culture flasks, detached by 2.5%/1% trypsin/EDTA (BioWhittacker Inc.), resuspended in fGMS, seeded (passage 5, 10 × 10^3 cells·$well^{-1}$) in 96-well flat-bottom microtiter plates, and cultured until confluence as described for HKs. fGMS was renewed or replaced with FITC-AC or $Ru(dpp)_3$-PAN in fGMS (0.1, 0.5, or 1.0 μg·mL^{-1}), and L929 were incubated for 48 h. Additionally, L929 (passage 5) were seeded on Thermanox slides (Nunc) in 24-well plates for (fluorescence) microscopic imaging.

HKs/L929 in 96-well plates were washed two times with kGMS/fGMS, and cytotoxicity was evaluated with the 3-(4,5-dimethyl-2-thiazolyl)-2,5-diphenyl-tetrazoliumbromide (MTT) assay. Supernatants were replaced by kGMS/fGMS supplemented with 16% MTT solution and incubated for 1–4 h (depending on absorbance). Reaction was stopped with 2% SDS, and triplet samples of absorbance were measured at 490 nm (reference wavelength = 650 nm, 96-well plate reader; MWG-Biotech). Cell viability was expressed as the percentage of viable cells compared with controls (kGMS/fGMS only).

Supernatants of L929 on 96-well plates after 24 and 48 h exposure to microparticles were analyzed for dead cell protease activity with CytoTox-Glo assays (Promega) according to the manufacturer's instructions. Luminescence counts were measured using a Victor^3 multilabel reader (PerkinElmer).

We examined the morphology of live HK/L929 monolayers (96-well plates) as well as particle exposure (96-, 24-, and 6-well plates) with an inverted (Labovert FS; Leica Microsystems) and a fluorescence microscope (Axiostar Plus; Carl Zeiss). For fluorescence microscopy, we used a 475/40-nm band-pass excitation filter and a 545/35-nm band-pass emission filter (Omega Optical).

Cellular Particle Uptake. For confocal microscopic imaging, L929 (passage 5, 50 × 10^3 cells·$well^{-1}$) were seeded on four-well Lab-Tek chamber slides (Nunc) and cultured until confluence. fGMS was replaced with microparticles in fGMS (1.0 μg·mL^{-1}), and L929 were incubated for 1 and 24 h, respectively. Supernatants were removed, and cells were embedded in paraformaldehyde (4%, 4 °C) for fixation and stored for 24 h until analysis. Subsequently, paraformaldehyde was removed, cells were washed three times with PBS plus Ca^{2+} plus Mg^{2+}, and membranes were stained with $DiC_{18}(3)$ (2 μg·mL^{-1} in PBS, 1 h incubation; Invitrogen). Supernatants were removed, cells were washed three times with PBS, and confocal microscopy was done with a Nikon Eclipse C-1/90i (Nikon Instruments) and a 488-nm laser (30-μm pinhole).

For electron microscopic analysis of the cellular uptake of microparticles, HKs (passage 6) were grown until confluence on 25-cm^2 culture flasks. kGMS was replaced with microparticles in kGMS (1.0 μg·mL^{-1}), and HKs were incubated for 24 h. HKs were detached (*Cytotoxicity*), resuspended in kGMS, and transferred to falcon tubes (BD Biosciences). Supernatants were removed from the cell pellets, and cells exposed to microparticles were embedded in Karnovsky's fixative for electron microscopy.

Singlet Oxygen Detection. Particle suspensions (Millipore water, 1 mg·mL^{-1}) were excited with a frequency-doubled Nd:YAG laser (532 nm, 100 × 10^3 pulses, 70-ns pulse duration, 100 mW, 20-s irradiation time, 8-mm spot size, and 2.0-kHz repetition rate; PhotonEnergy). Suspensions were magnetically stirred. We investigated singlet oxygen luminescence with an IR-sensitive photomultiplier (R5509-42; Hamamatsu Photonics). The luminescence signal was detected by means of a 950-nm cutoff filter (Omega Opticals) and a 1,270-nm bandpass filter with a full

width of half-maximum (FWHM) of 10 nm (LOT-Oriel). To analyze data, we used Mathematica 5.2 (Wolfram Research).

Study Subjects. All participants were provided with verbal and written information on the study, and signed informed consent was obtained from each participant. The local ethics committee gave approval (No. 06/171: 2007), and all experiments were conducted in full accordance with the sixth revision (Seoul, Korea, 2008) of the Declaration of Helsinki (1964). For the stratum corneum (SC) tape-stripping experiments, male volunteers ($n = 10$; 27.7 ± 4.0 y) were included. None of the volunteers had any history of skin disorders, had suffered from a skin condition, or had been subject to dermatological treatment on the volar forearm in the past or at the time of measurement. Volunteers did not exercise, wash, or apply topical formulations on the volar forearm for 24 h before the measurements. Split-skin grafts (thickness = 400 μm, $n = 10$, 4/6 female/male, 65.10 ± 20.23 y) were harvested from the left or right thigh to cover tissue defects at different body sites after excision of skin tumors. A chronic venous ulcer on the medial right ankle of a female patient (66 y) was visualized.

Statistics. We used Sigma Plot 11.0 (Systat Software Inc.) for all analyses. Data are given as mean ± SD except when otherwise denoted. Normality testing was passed, and paired t tests were done to analyze differences between pH values during the time course of split-skin donor-site healing. We conducted t tests to check for differences between the measurements obtained by luminescence imaging and glass electrodes. We considered a P value below 0.05 as significant and a P value below 0.01 as highly significant. Results were marked with one or two asterisks within the graphs. To assess the precision of the methods, we calculated the relative SD (RSD) of measurements as $(SD \cdot mean^{-1}) \times 100\%$. For method comparisons, we created Bland–Altmann mean difference plots for pH measurements and calculated the respective Krippendorf coefficients K.

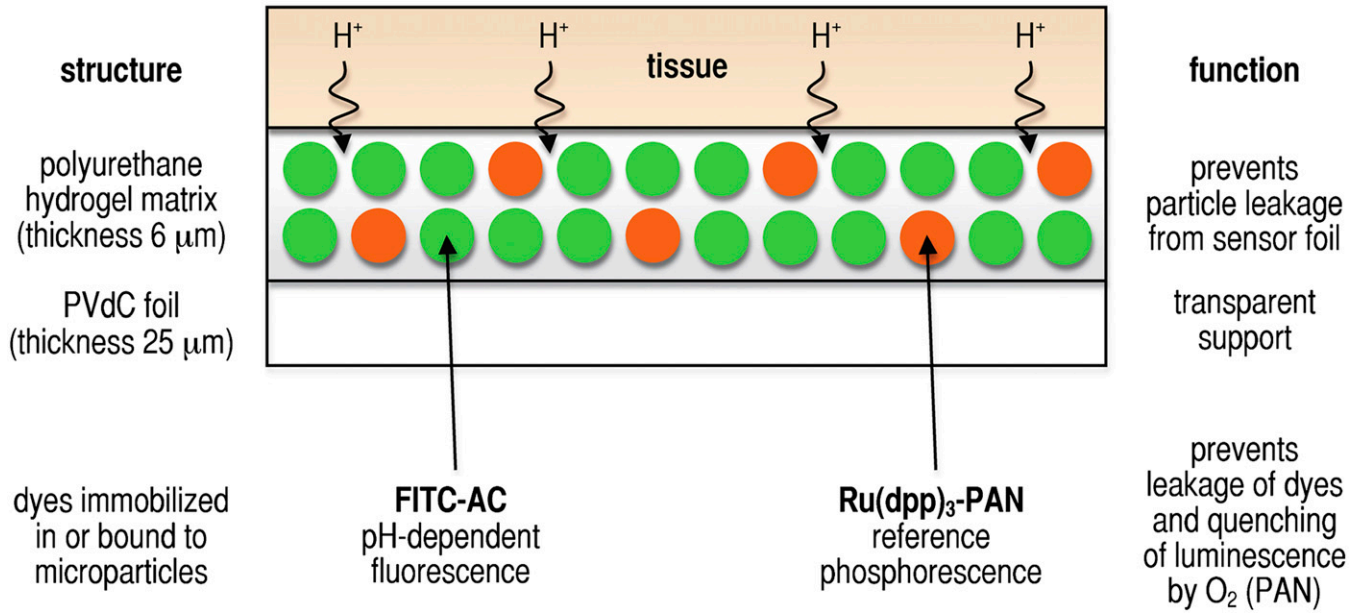

Fig. S1. Sensor foil structure. A schematic view of a sensor foil is shown. Particles are embedded in a hydrogel matrix on transparent poly(vinylidene-chloride) (PVdC) foils, thereby preventing particle leakage. Foils are applied to tissues with the hydrogel-coated surface. Protons diffuse into the hydrogel matrix and to the microparticles. The transparency of the foils allows simultaneously observing the underlying anatomic structures.

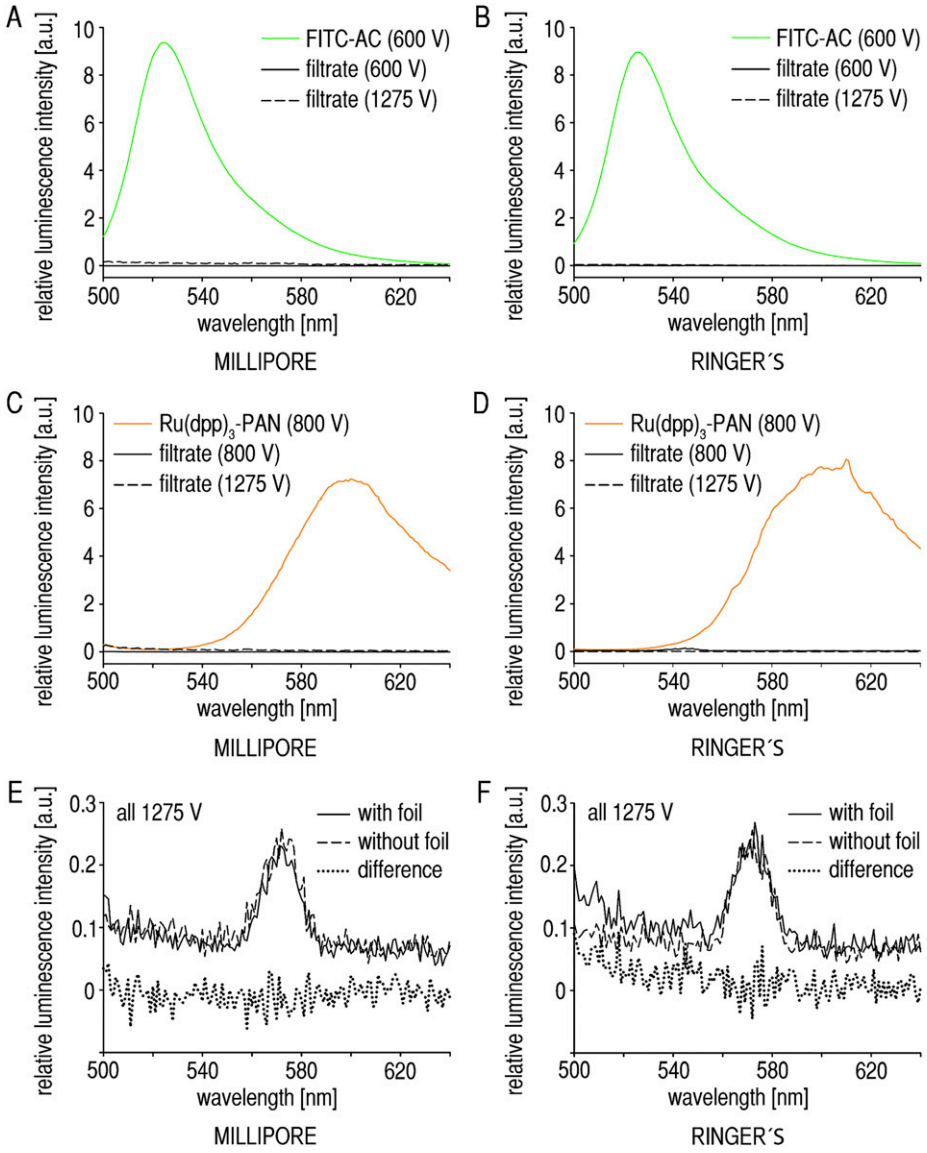

Fig. S2. Leaching of dyes and particle leakage. (*A–D*) Results of leaching experiments for both dyes in Millipore water and Ringer's solution. Colored lines represent the luminescence spectra of the particle suspension, and solid black lines equal the spectra of the centrifuged and filtered solutions with constant detector gain. Dashed lines (full detector gain) show the lack of dye traces in filtered solutions. Thus, no leaching of dyes out of the particles occurred (a.u., arbitrary units). (*E* and *F*) Results of experiments on particle leakage out of the sensor. The spectra of the incubated solution (solid lines) and blank controls (dashed lines) are given. The peak at 570 nm results from an internal reflection in the instrument. The corrected spectra (dotted lines) indicate no leakage of FITC-AC and $Ru(dpp)_3$-PAN into both solutions (a.u., arbitrary units).

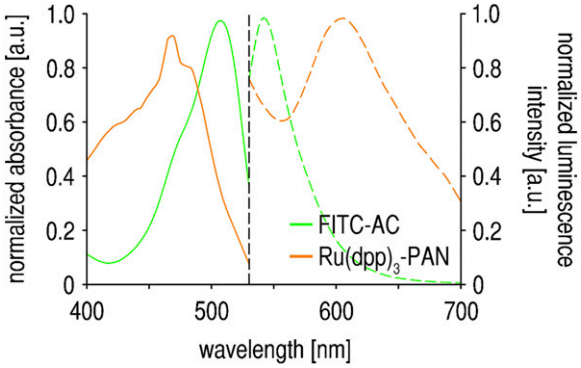

Fig. S3. Absorbance and luminescence emission spectra of the sensor. Solid lines represent absorbance, and dashed lines represent luminescence intensity. Luminescence intensity was measured with 460-nm excitation. The vertical dashed line symbolizes the 530-nm long-pass optical filter used for in vitro and in vivo luminescence intensity detection (a.u., arbitrary units).

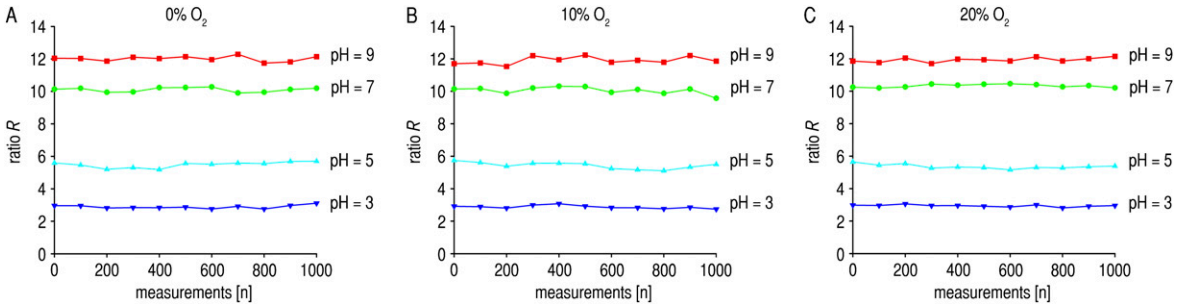

Fig. S4. Luminescence intensity ratios at varying oxygen and pH values. The ratio *R* of the luminescence intensities of FITC and $Ru(dpp)_3$ is presented for 1,000 repetitive measurements under (*A*) 0%, (*B*) 10%, and (*C*) 20% oxygen. For each oxygen concentration, data on *R* are presented for varying pH values. There is virtually no change in *R* for each of the conditions studied.

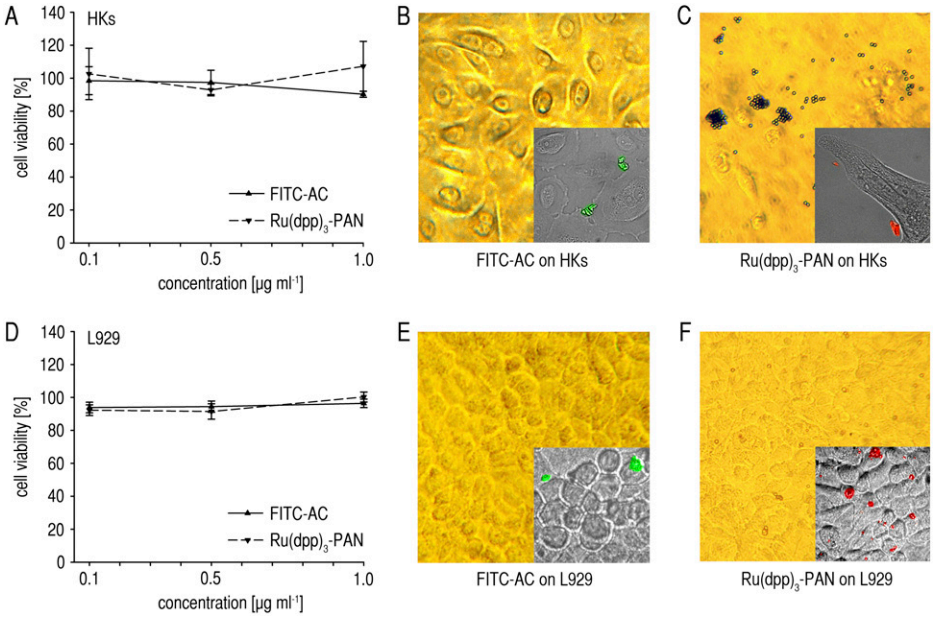

Fig. S5. MTT and particle exposure. (*A* and *D*) No cytotoxicity of FITC-AC and $Ru(dpp)_3$-PAN to (*A*) HKs and (*D*) L929 fibroblasts was observed as quantified by MTT assays. Cell viability is expressed as the percentage of viable cells compared with controls (mean ± SEM; triplicate samples). (*B* and *E*) FITC-AC particles are only visible using fluorescence microscopy (green in *Insets*). (*C* and *F*) Inverted and fluorescence microscopy shows the exposure of HKs/L929 to $Ru(dpp)_3$-PAN particles (dark colored circles; red in *Insets*). As seen in *C Inset* and *F Inset*, both particle types tend to agglomerate and are not taken up by live HKs/L929 (Figs. S7 and S8 and Movies S2–S5).

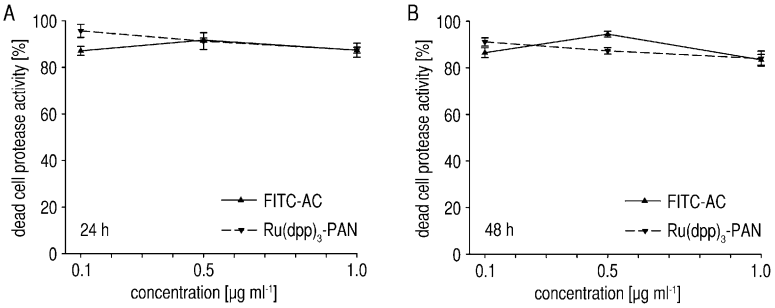

Fig. S6. Dead cell protease release. No increase in dead cell protease release from L929 was observed after (*A*) 24 and (*B*) 48 h, indicating that particles exhibit no cytotoxic potential. Dead cell protease activity is given as the percentage of untreated controls (controls: 4,687 ± 207 counts·s^{-1} after 24 h and 4,820 ± 50 counts·s^{-1} after 48 h; mean ± SEM, triplicate samples).

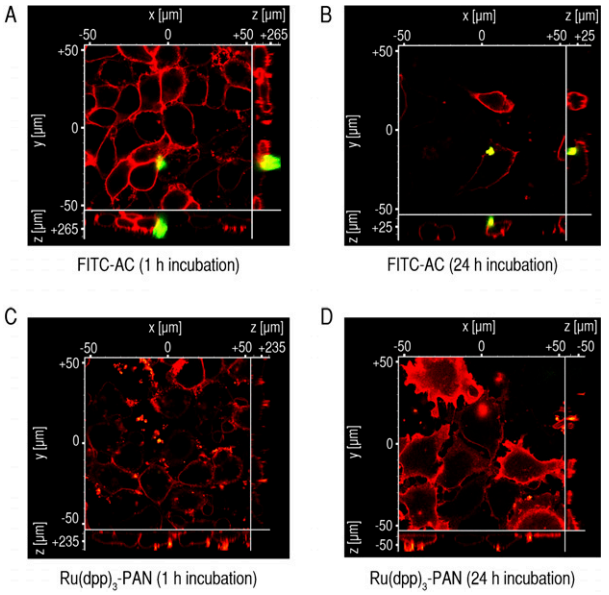

Fig. S7. Confocal microscopic analysis of cellular particle uptake. (*A–D*) Neither FITC-AC nor $Ru(dpp)_3$-PAN particles (both 1.0 µg·mL^{-1} in supernatants) is taken up by live L929 fibroblasts after (*A* and *C*) 1 and (*B* and *D*) 24 h incubation. (*A* and *B*) FITC-AC is shown (green) as particle agglomerates on the cell surface. (*C* and *D*) Multiple $Ru(dpp)_3$-PANs are shown (yellow to orange) on the surface of various cells. For better visualization, see confocal microscopic image stacks in Movies S2–S5.

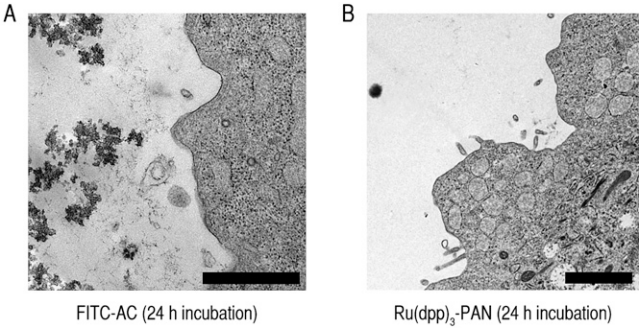

Fig. S8. Electron microscopic analysis of cellular particle uptake. Neither FITC-AC (*A*) nor $Ru(dpp)_3$-PAN (*B*) are taken up by live HKs. (*A*) FITC-AC agglomerates are seen in the left part of the image in close proximity to HKs. No FITC-AC could be found inside HKs. (*B*) A single $Ru(dpp)_3$-PAN particle is shown outside live HKs in the left part of the image. $Ru(dpp)_3$-PAN was not found inside HKs. (Scale bars, *A*, 1 µm; *B*, 2 µm).

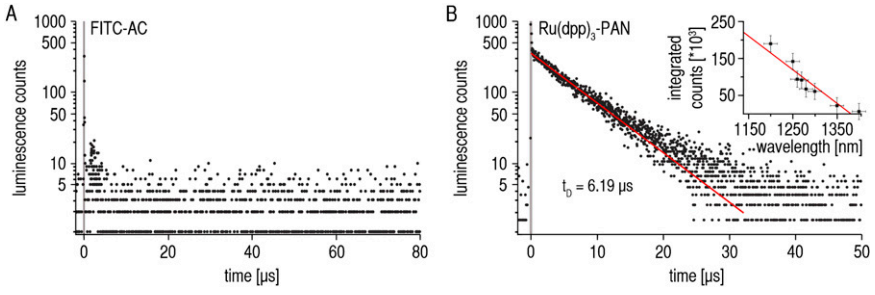

Fig. S9. Singlet oxygen detection. Neither (*A*) FITC-AC nor (*B*) $Ru(dpp)_3$-PAN led to the formation of singlet oxygen. (*A* and *B*) 0 µs denotes the start of excitation (vertical gray lines). (*B*) The red line shows the exponential decay of luminescence (t_D = decay time), representing the phosphorescence signal of $Ru(dpp)_3$-PAN. *Inset* shows the integrated luminescence signal at certain wavelengths (fit shown as red line).

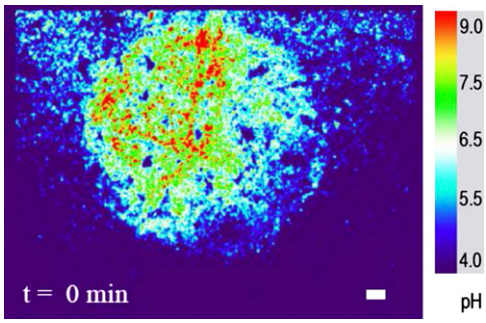

Movie S1. Spatiotemporal resolution shown by real-time microscopic 2D pH imaging. Spatial resolution shown by a representative visualization of a drop (pH 8) on a sensor foil impregnated in a solution of pH 4 after connecting the charge-coupled device (CCD) camera to a microscope. To assess whether significant horizontal proton diffusion exists that affects spatial resolution, continuous imaging was conducted (images were acquired every 2 min in the first 20 min and then after 30 min). No significant change was found in the spatial aspect of pH values. Resolution was found to be <5 μm. For additional data on the time response of the sensor, see Fig. 2 *E* and *F*. (Scale bar, 10 μm.)

Movie S1

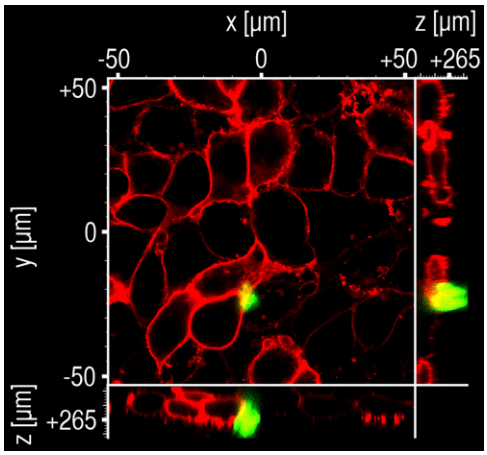

Movie S2. Confocal microscopy of cells exposed to FITC-AC (1 h). Confocal microscopic image stack of L929 fibroblasts exposed to FITC-AC for 1 h. FITC-AC (green) is only found on the cell surface, not inside live L929 fibroblasts. In the static *z* scale, the location of the particle is additionally visualized.

Movie S2

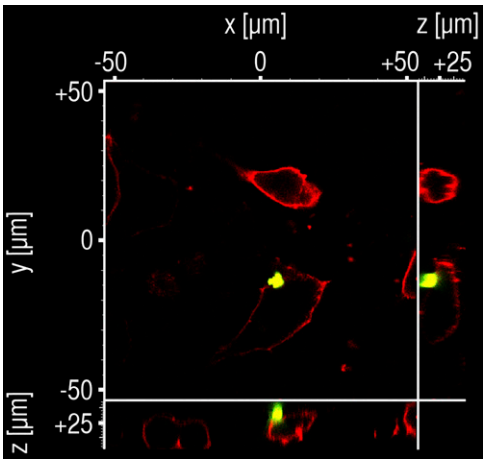

Movie S3. Confocal microscopy of cells exposed to FITC-AC (24 h). Confocal microscopic image stack of L929 fibroblasts exposed to FITC-AC for 24 h. FITC-AC (green) is only found on the cell surface, not inside live L929 fibroblasts. In the static *z* scale, the location of the particle is additionally visualized.

Movie S3

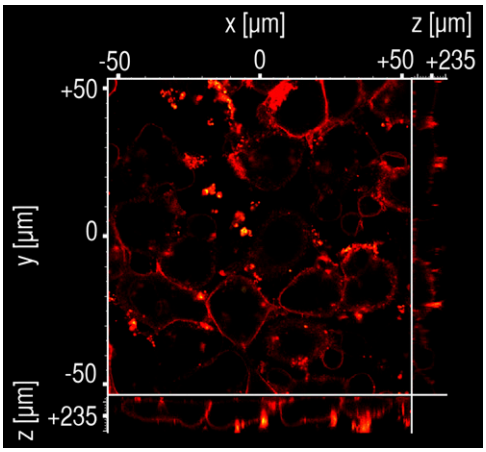

Movie S4. Confocal microscopy of cells exposed to $Ru(dpp)_3$-PAN (1 h). Confocal microscopic image stack of L929 fibroblasts exposed to $Ru(dpp)_3$-PAN for 1 h. $Ru(dpp)_3$-PAN (yellow to orange) is only found on the cell surface, not inside live L929 fibroblasts. In the static *z* scale, multiple particles on the cell surfaces are additionally visualized.

Movie S4

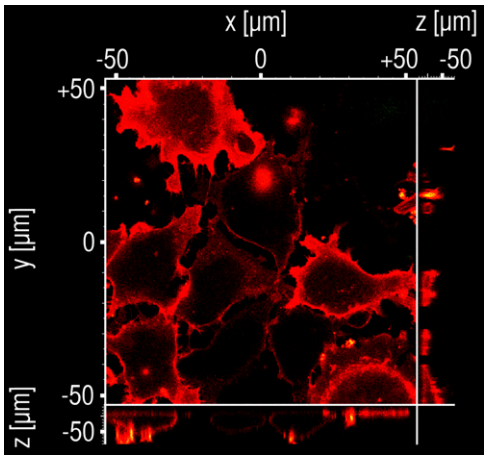

Movie S5. Confocal microscopy of cells exposed to $Ru(dpp)_3$-PAN (24 h). Confocal microscopic image stack of L929 fibroblasts exposed to $Ru(dpp)_3$-PAN for 24 h. $Ru(dpp)_3$-PAN (yellow to orange) is only found on the cell surface, not inside live L929 fibroblasts. In the static *z* scale, multiple particles on the cell surfaces are additionally visualized.

Movie S5